ARTICLE NO. 78-1357R

Fluctuating Pressures on Mildly Indented Nosetips

J. Peter Reding*
Lockheed Missiles & Space Company, Inc., Sunnyvale, Calif.

Fluctuating pressure measurements at $M=5.0$ are presented for turned (axisymmetric) nose shapes that represent approximations of cross sections (at various meridians) of the recovered graphite nosetip of the Nosetip Recovery Vehicle (NRV). Selected fluctuating pressure measurements are also presented for a replica of the NRV nosetip and a replica of a wind-tunnel-ablated camphor nosetip that roughly resembles the NRV nosetip. The greatest fluctuating pressures occurred under imbedded shock waves and/or the reattachment shock waves of imbedded regions of separated flow. The nondimensionalized power spectra under the reattachment shocks are in good agreement with similar measurements for spiked cones and a drag-reduction spike. Evidence of a Reynolds number sensitive resonant peak was observed in the spectra under reattachment on the NRV nose due to surface irregularities.

Nomenclature

a	= speed of sound, in./s
C_P	= pressure coefficient $= (p-p_\infty)/q$
$C_{P(\text{rms})}$	= root-mean-square fluctuating pressure coefficient $= \Delta p_{(\text{rms})}/q$
D	= nosetip reference diameter, in.
f	= frequency, Hz
M	= Mach number $= U/a$
PSD	= power spectral density, $(\text{psi})^2/\text{Hz}$
p	= local pressure, psi
p_∞	= freestream static pressure, psi
$p(t)$	= time varying pressure, psi
$\Delta p_{(\text{rms})}$	= fluctuating pressure $= \left[\frac{1}{T}\int_0^T p(t)^2 dt - p^2\right]^{1/2}$, psi
q	= freestream dynamic pressure $= pU^2/2$, psi
R_e	= freestream Reynolds number, ft^{-1}
U	= freestream velocity, in./s
X	= axial coordinate, in.
α	= angle of attack, deg
δ_m	= maximum separated flow height, in.
ρ	= freestream density, $\text{lb sec}^2/\text{in.}^4$

Introduction

DURING re-entry the initially spherical nose of the re-entry vehicle flattens due to ablation caused by laminar heating in the vicinity of the stagnation region. This is followed by a blunt conic shape as transition moves onto the sides of the nosetip causing increased ablation locally. As the aggravated ablation, caused by transition, persists on the sides of the nosetip, cusping occurs. Cusping develops differently around the nosetip due to random perturbations of the transition front or material inhomogeneities or both. Thus, blunt conic and cusped cross sections may occur simultaneously along different meridians as observed on wind-tunnel ablated models (Fig. 1).[1] Furthermore, the longitudinal ridges observed on the recovered graphite nosetip of the Nosetip Recover Vehicle (NRV) are probably remnants of blunt conic sections that were once interspersed with cusped sections (Fig. 2)[2]. Eventually the nosetip becomes extremely indented and resembles a spiked cone or a "tension shell" body. Finally, the spike is lost and the nosetip becomes roughly conic.

Fluctuating pressure measurements have been obtained on tension shell[3] and spiked bodies[4-6] that approximate severely indented nosetips. The separated flows for these configurations have exhibited violent periodic flow oscillations and/or large flow pulsations that result in very large periodic surface pressure fluctuations. For certain of these geometries, those with the so-called steady separated flow, large random pressure fluctuations have been measured. There has, however, been a paucity of information on the mildly indented nosetips that are characteristic of the recovered graphite (NRV) nosetip.[2] The following presents fluctuating pressure measurements for turned (axisymmetric) nose shapes (Fig. 3) that represent approximations of cross sections (at various meridians) of the NRV nose (Fig. 2)[2] and a replica of a wind-tunnel-ablated camphor nose (Fig. 1)[1]. Also selected fluctuating pressure measurements are presented for the NRV nose, the replica of the low-temperature ablator (LTA) or camphor nose and a smoothed replica of the LTA nose. The smoothed LTA replica model was identical to the LTA replica, except that local surface scallops were filled in. These scallops are typical of camphor, but not of graphite nosetips. Thus, the smoothed LTA replica model better simulates actual flight vehicle nosetips.

Wind-Tunnel Tests

The wind-tunnel test was conducted in Tunnel 8 of the Naval Surface Weapons Center, White Oak Laboratory, at $M=5.0$ and over a Reynolds number range $10\times10^6/\text{ft} \le Re \le 40\times10^6/\text{ft}$.[7] The fluctuating pressures were measured with Kulite fluctuating pressure transducers (located as shown in Figs. 1-3) that had a 70,000-Hz resonant frequency. The models were initially supplied with additional transducers; however, these were lost during the test for a variety of reasons such as, overpressurization (static pressure), overheating (despite water cooling of the model), and impacts by tunnel contaminants.

Data were recorded over the frequency range of 200 to 40,000 Hz and reduced in 250-Hz bandwidths. Some of the

Presented as Paper 78-1357 at the AIAA Atmospheric Flight Mechanics Conference, Palo Alto, Calif., Aug. 7-9, 1978; submitted Aug. 31, 1978; revision received April 17, 1979. Copyright © American Institute of Aeronautics and Astronautics, Inc., 1978. All rights reserved. Reprints of this article may be ordered from AIAA Special Publications, 1290 Avenue of the Americas, New York, N.Y. 10019. Order by Article No. at top of page. Member price $2.00 each, nonmember, $3.00 each. **Remittance must accompany order.**

Index categories; Entry Vehicle Testing, Flight and Ground; Aeroacoustics; Jets, Wakes, and Viscid-Inviscid Flow Interactions.

*Research Specialist. Member AIAA.

TRANSDUCER	X	Ø
F_1	.200D	0
F_2	.316D	60°
F_3	.083D	180°
F_4	.098D	192°

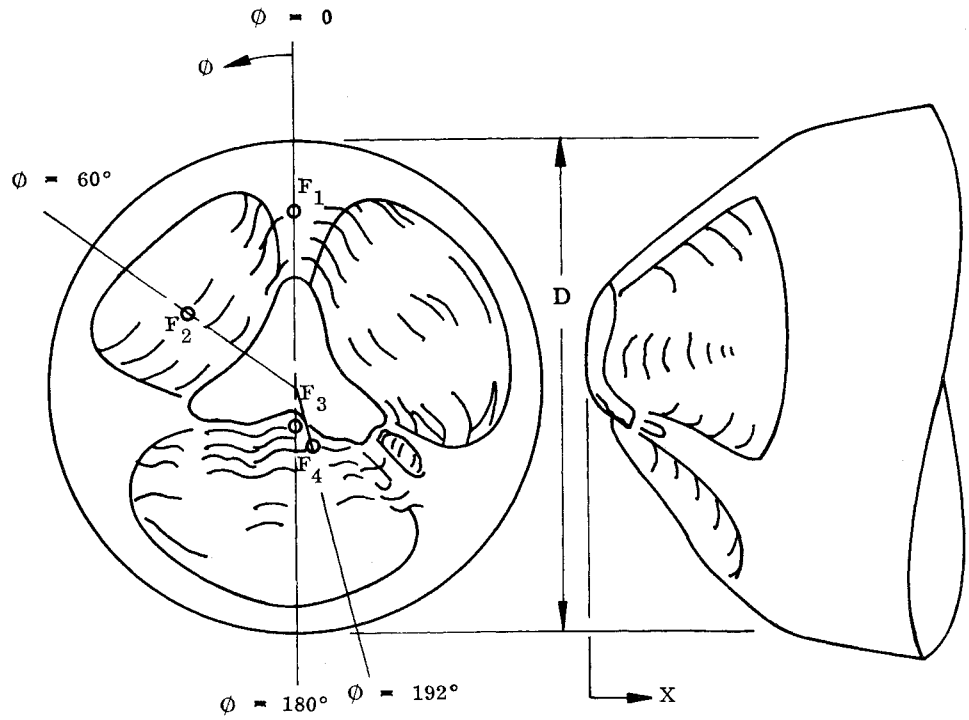

Fig. 1 LTA replica (smooth and rough), wind-tunnel-ablated camphor nosetip.

TRANSDUCER	X	Ø
F_1	.28D	310°
F_2	.14D	295°
F_3	.28D	180°

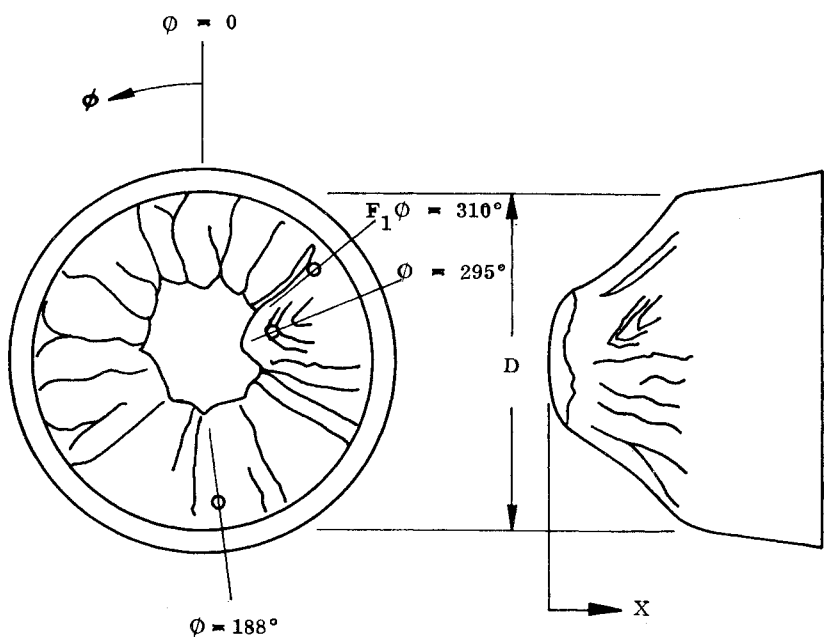

Fig. 2 NRV, recovered graphite nosetip.

measurements were swamped by background noise. The data were judged valid if the power spectra were at least one order of magnitude above the background noise. Of course, the background noise could not be removed from the signal since the phase relationship between the two is unknown. A typical example of valid data appears in Fig. 4.

The models were the same models used in previous static pressure and force tests.[8-10] Good Reynolds number simulation was essential since it was known from the previous tests that flow separation would occur on most of the models. Although Ref. 11 showed that transition locations very near the stagnation point are possible in Tunnel 8 for $R_e \geq 20 \times 10^6$/ft, there was still concern that transitions might occur downstream of the laminar cap in the separated region resulting in transitional reattachment. Thus, the models were tested over a Reynolds number range up to the maximum practical Reynolds number of 40×10^6/ft.

Overall Fluctuating Pressures

Overall fluctuating pressure coefficient measurements, $C_{P(rms)}$ are compared with static pressure measurements[3,9,12] and with flow sketches (traced from shadowgraph photographs) in Figs. 5-13. Flow separation was positively observed to occur in the shadowgraph photographs of models 3 and 4 only. Whether or not flow separation occurred on model 2 could not be positively determined from the shadowgraphs; therefore, the flow sketch in Fig. 8 does not show flow separation though it may have been present. Separation undoubtedly occurred on the NRV and LTA (smooth and rough) noses although the asymmetric nature of the noses and the multitude of shock waves emanating from the various roughness elements precluded quantitative observation of the separated flow regions. Thus, the separated regions sketched in Figs. 9-12 were inferred from the static pressure data.

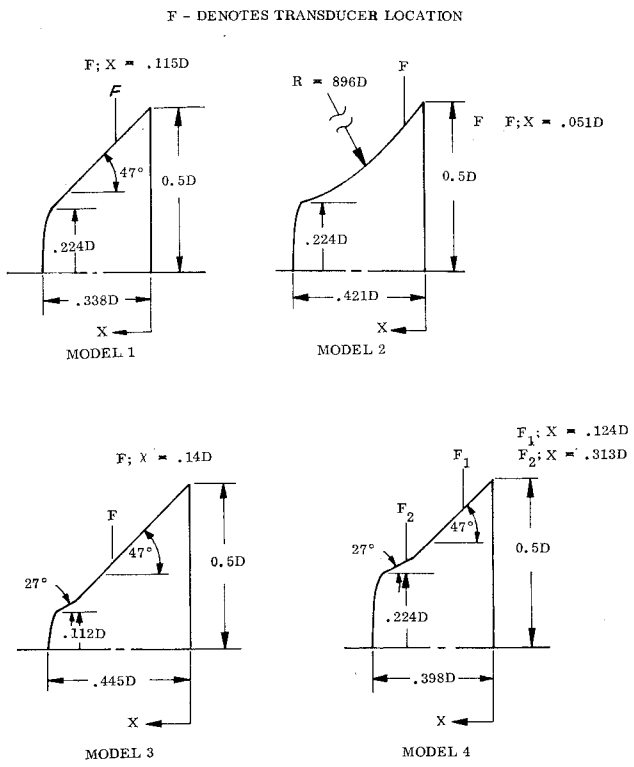

Fig. 3 Axisymmetric nosetips.

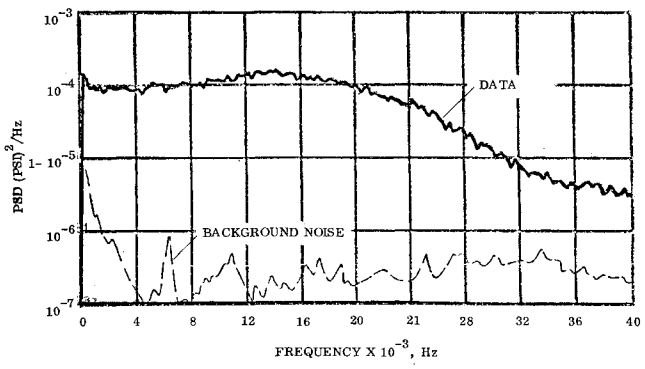

Fig. 4 Typical background noise comparison, valid data.

Uniform flow cone pressures are not achieved on the blunt conic model due to the entropy wake behind the bow shock (Fig. 5)[13]; however, when flow separation is present on the indented noses, the static pressures due to reattaching separated flow often exceed the cone value (Figs. 6-12). The location of the imbedded reattachment shocks correlates with the large adverse static pressure gradient produced by the reattaching separated flow. It is believed that reattachment is not complete until the peak static pressure is realized. Fluctuating pressure transducers were located both under the separated flow and reattachment regions, as indicated by both shadowgraph photographs and static pressure data. Unfortunately, no static pressure data were available on the NRV nosetip at $M=5.0$. Thus, the $M=11.3$ data from Ref. 12 are presented in Figs. 9 and 10; however, it is believed that the location of the reattachment region is not substantially different between $M=5.0$ and $M=11.3$.

Generally the only significant Reynolds number effect occurred at $R_e=10\times10^6$/ft under the separated region of model 4 (Fig. 7). Here the overall fluctuating pressures are more than double those measured at the higher Reynolds numbers. This appears to be a combined effect of flow

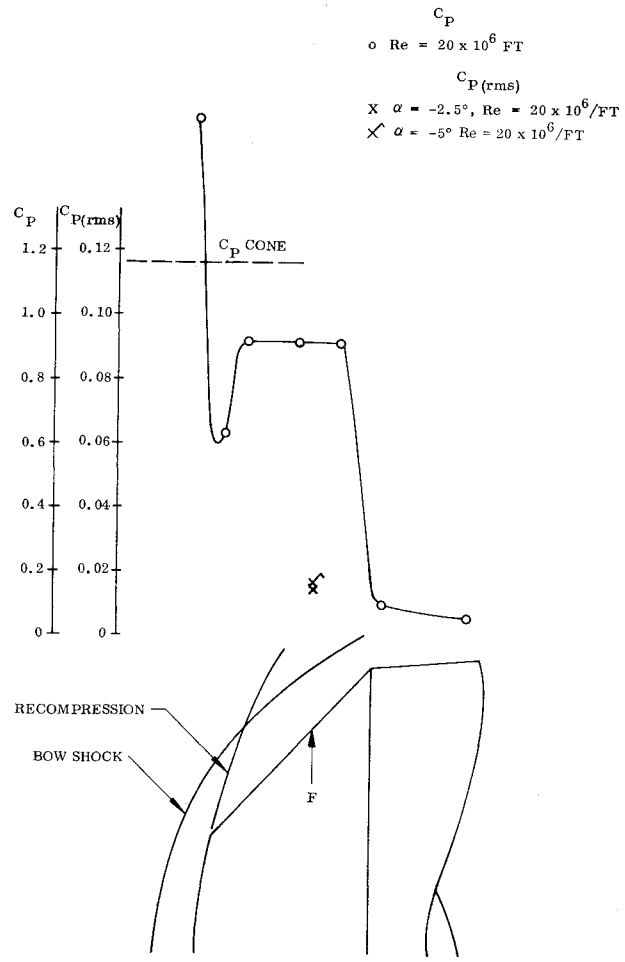

Fig. 5 Comparison of static and fluctuating pressures for model 1, $M=5.0$.

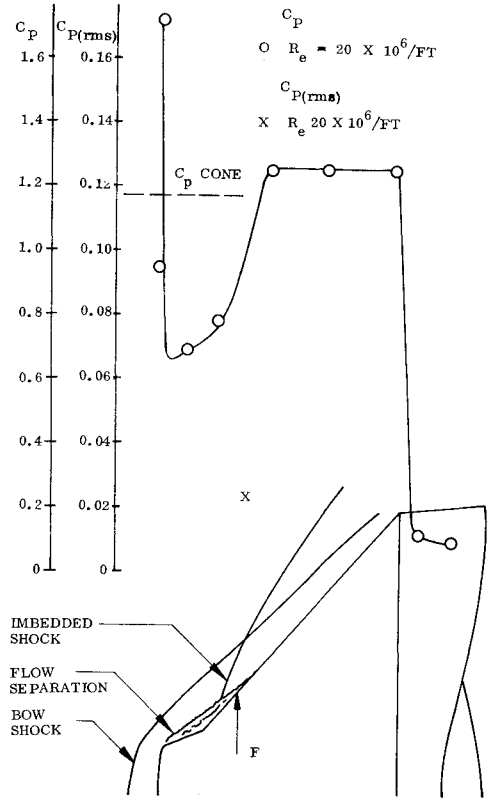

Fig. 6 Comparison of static and fluctuating pressures for model 3, $M=5.0$, $\alpha=0$ deg.

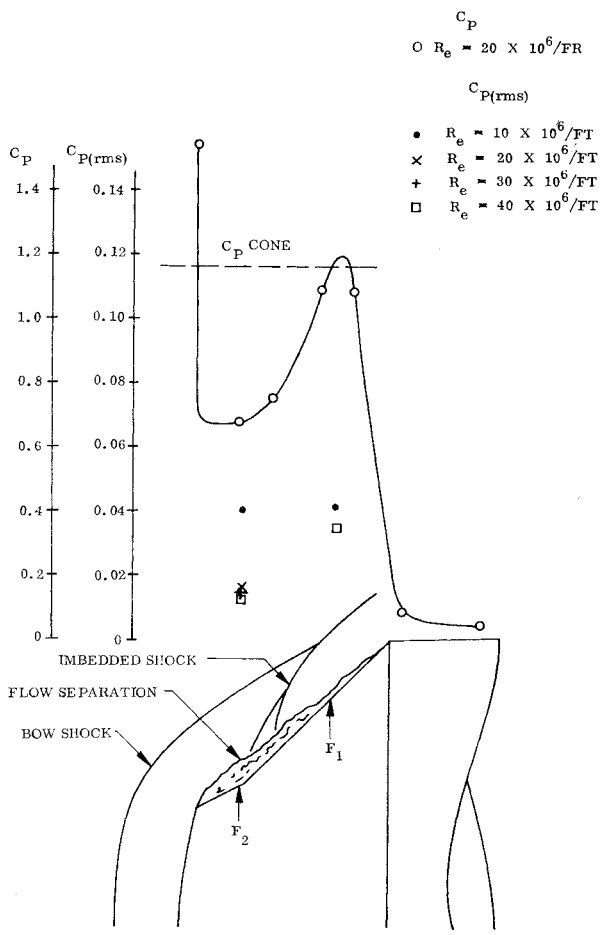

Fig. 7 Comparison of static and fluctuating pressures for model 4, $M = 5.0$, $\alpha = 0$ deg.

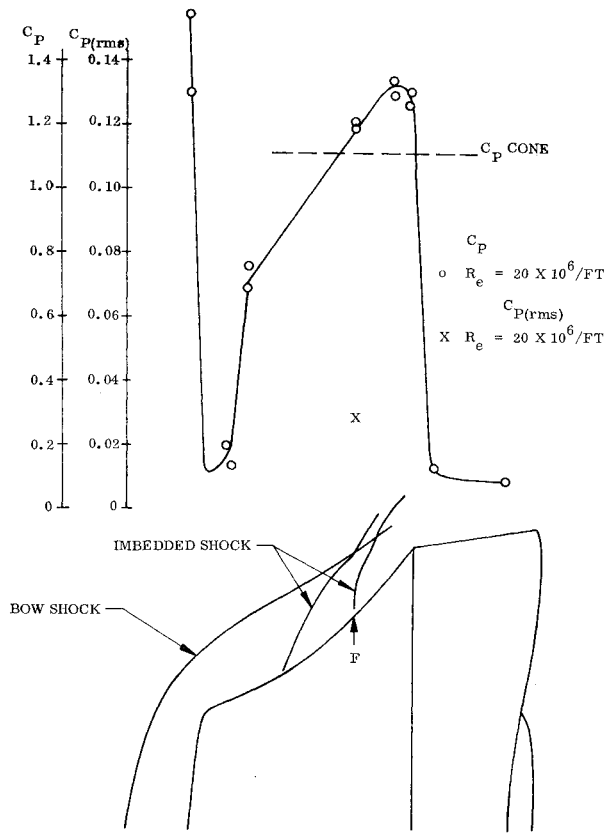

Fig. 8 Comparison of static and fluctuating pressures for model 2, $M = 5.0$, $\alpha = 0$ deg.

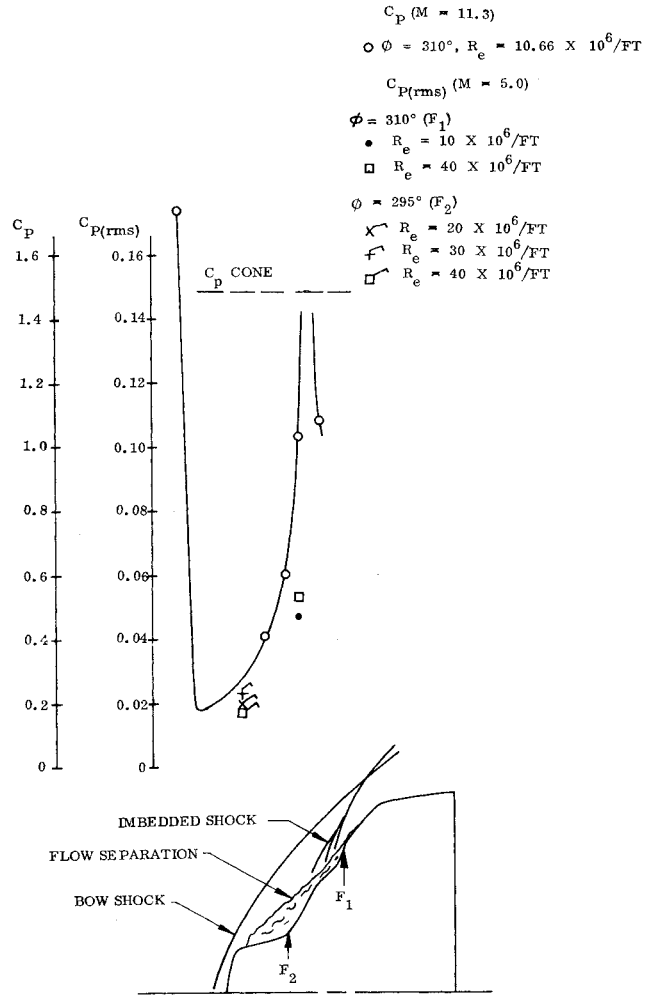

Fig. 9 Comparison of static and fluctuating pressures for the NRV nose, $\phi = 311$ deg.

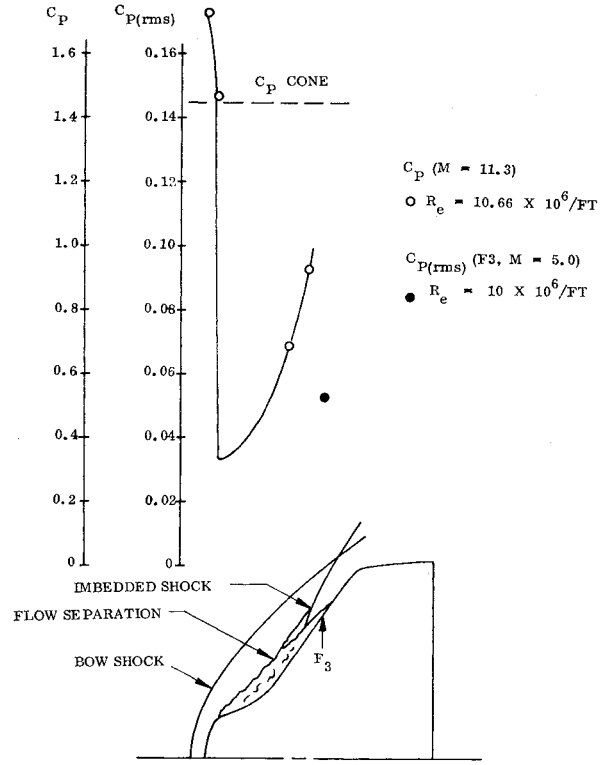

Fig. 10 Comparison of static and fluctuating pressures for the NRV nose, $\phi = 188$ deg.

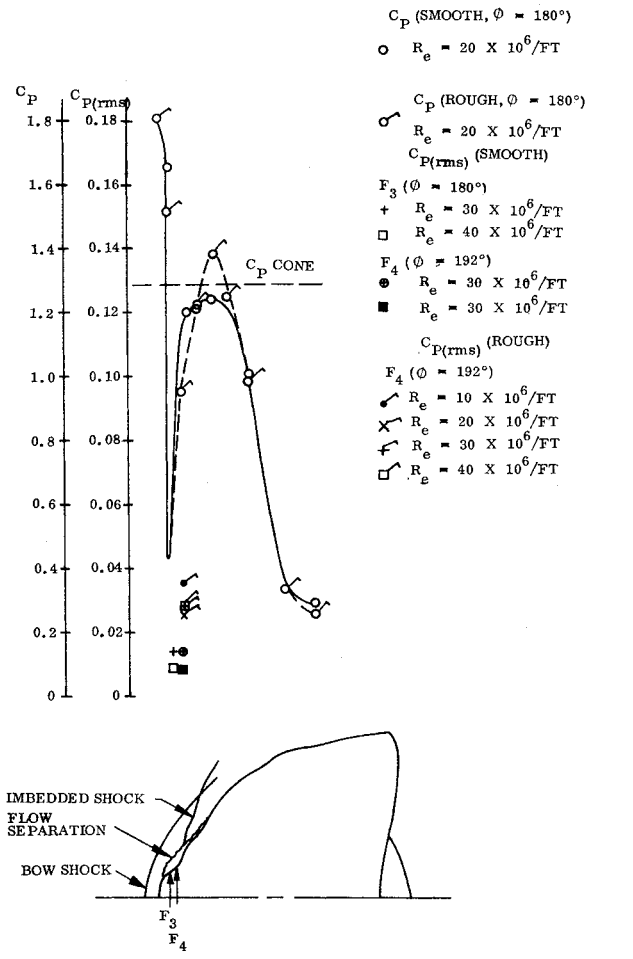

Fig. 11 Comparison of static and fluctuating pressures for the LTA nose, $M = 5.0$.

resonance and transitional flow separation, as will be discussed later.

The effects of surface roughness are evident in both the static and fluctuating pressure measurements on the two LTA models (smooth and rough). The most significant effect occurs along the $\phi = 192$-deg meridian (Fig. 11). The F_4 transducer was located in the bottom of a local scallop or small cavity under the separated region of the rough LTA model; whereas the cavity was smoothed over on the smooth model. The local cavity effect caused a 2 to 3 times increase in the overall fluctuating pressure (depending on the Reynolds number) even though it was located under the separated region.

The static pressure distribution along the blunt conic ($\phi = 0$ deg) meridian of the LTA replica models is quite different from the distribution along the axisymmetric blunt conic model although the fluctuating pressures are about the same (compare Figs. 5 and 13). The static pressure overshoots the cone value, and the pressure distribution on the LTA replica generally resembles the distribution along a meridian where flow separation exists. Evidently, the reattachment shocks from the adjacent separated regions (e.g., the $\phi = 60$-deg meridian, Fig. 12) extend laterally affecting the pressures along the $\phi = 0$-deg meridian although the flow there is attached.

The fluctuating pressures measured in flow reattachment regions from the present test correlate nicely with other measurements taken in the reattachment region of a variety of separated flows (Fig. 14). It is interesting that the present results agree better with those from the 45-deg conic frustum,[14,15] a flow separation spike,[16,17] and the reattaching wake from the Apollo escape rocket[18] than they do with data from a spiked cone that was intended to simulate an indented nosetip.[6] The relative insensitivity of the overall fluctuating pressures at reattachment to spike configuration and length is surprising since spike length is an important parameter in establishing the stability boundaries for spike-induced

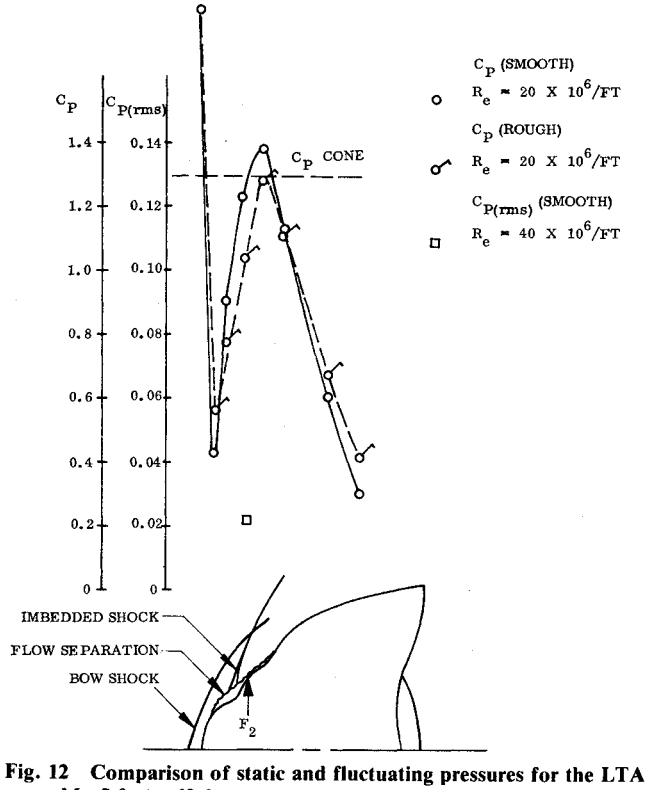

Fig. 12 Comparison of static and fluctuating pressures for the LTA nose, $M = 5.0$, $\phi = 60$ deg.

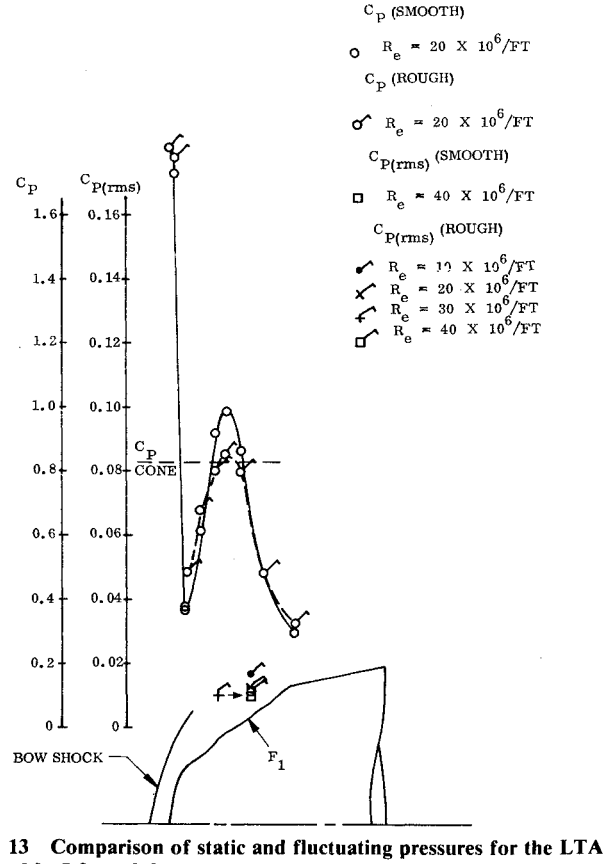

Fig. 13 Comparison of static and fluctuating pressures for the LTA nose, $M = 5.0$, $\phi = 0$ deg.

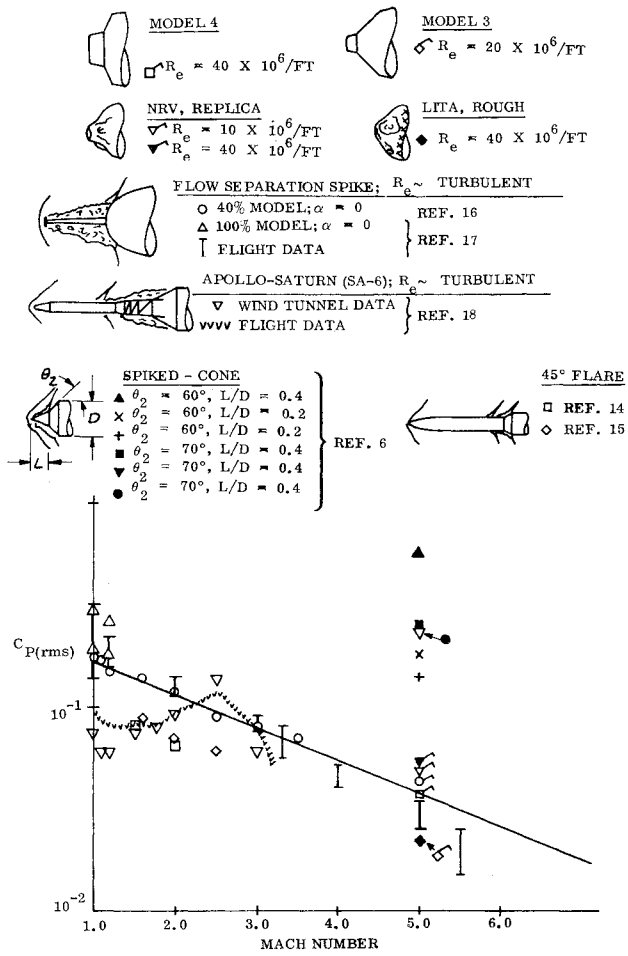

Fig. 14 Comparison of fluctuating pressure levels at reattachment.

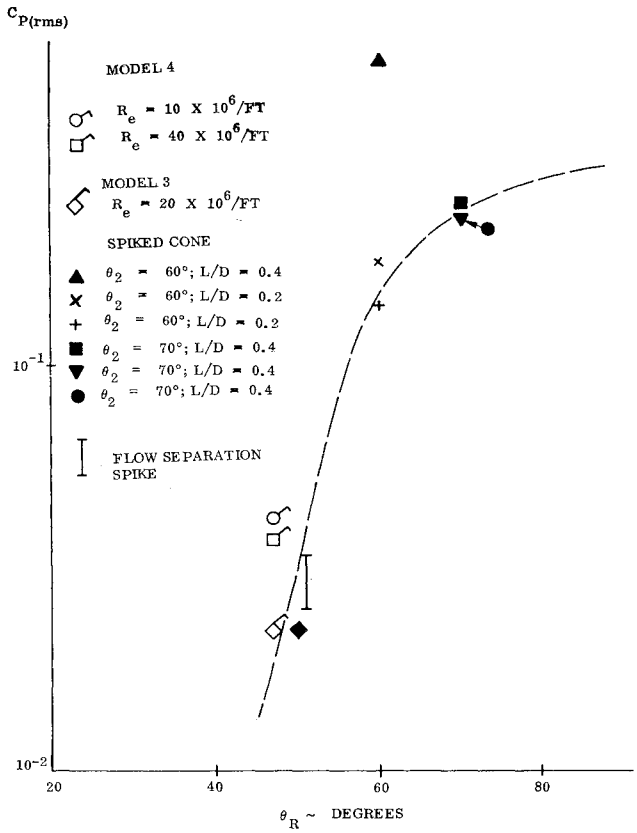

Fig. 15 Effect of body slope at reattachment on the overall fluctuating pressures at reattachment, $M = 5.0$.

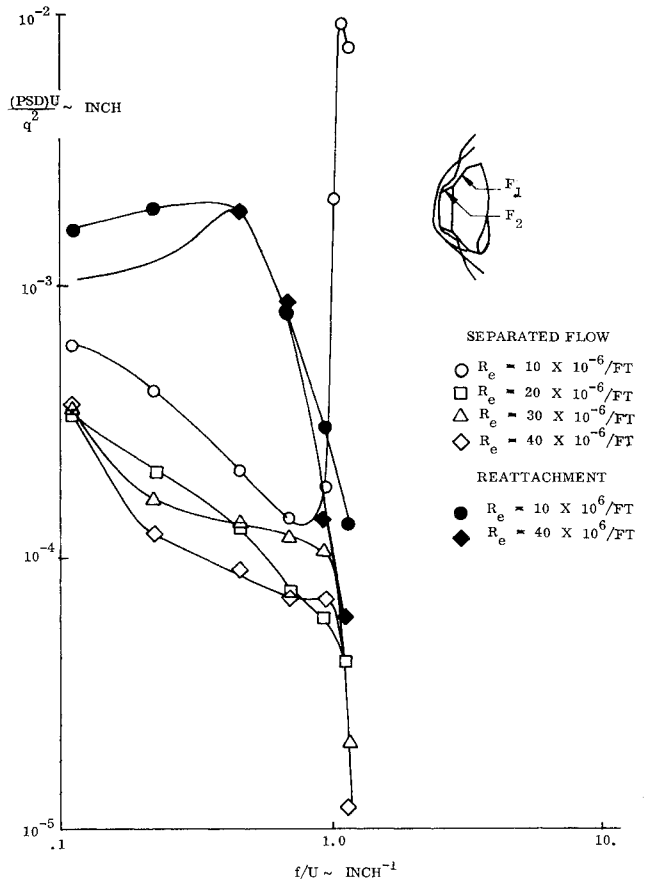

Fig. 16 Comparison of separated flow spectra, model 4, $\alpha = 0$ deg, $M = 5.0$.

separated flows.[4,6,19] Correlation of the overall fluctuating pressures in the reattachment region at $M = 5.0$ indicates a significant effect of body slope on the magnitude of the fluctuating pressures at reattachment (Fig. 15). This is not surprising, since body slope is also an important parameter in determining the stability of spike body flows.[4,5]

Power Spectra

Semi-normalized power spectra are presented in Fig. 16 for model 4.† There is a distinct difference in the shape as well as the level of the spectra between the separated flow region and the reattachment region. There is also a resonant peak in the separated flow spectra for $R_e = 10 \times 10^6$/ft which partially explains why the overall fluctuating pressure level is greater at $R_e = 10 \times 10^6$/ft than for other Reynolds numbers as discussed earlier (Fig. 7).

Is is hard to understand how a flow resonance could exist under the separated region and not be reflected in the reattachment spectra. However, a critical examination of the data for the F_2 transducer on model 4 gives no reason to doubt the veracity of the measurements since no anomaly could be found in the data from other tests, in the calibration data, in the model response as measured by accelerometers or in the data reduction.

The general level of the spectra under the flow separation at $R_e = 10 \times 10^6$/ft is above the higher Reynolds number spectra (Fig. 16). This may be indicative of transitional separation at $R_e = 10 \times 10^6$/ft. Martellucci et al.[20] have shown that the fluctuating pressure spectra under transitional and turbulent boundary layers have the same shape, although the level of

†The data points in Fig. 16 and the other spectra plots are only for identification of the spectra. They are not indicative of bandwidth center frequencies.

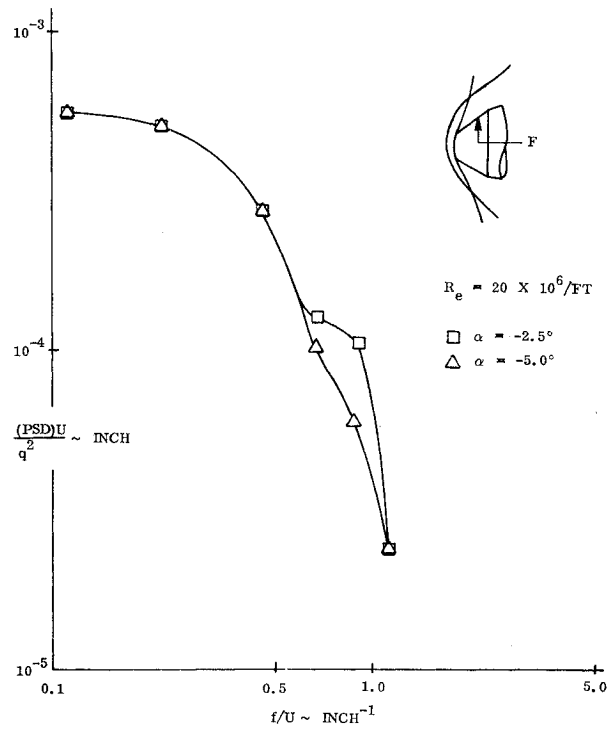

Fig. 17 Attached flow spectra on blunt conic nose, model 1, $M = 5.0$.

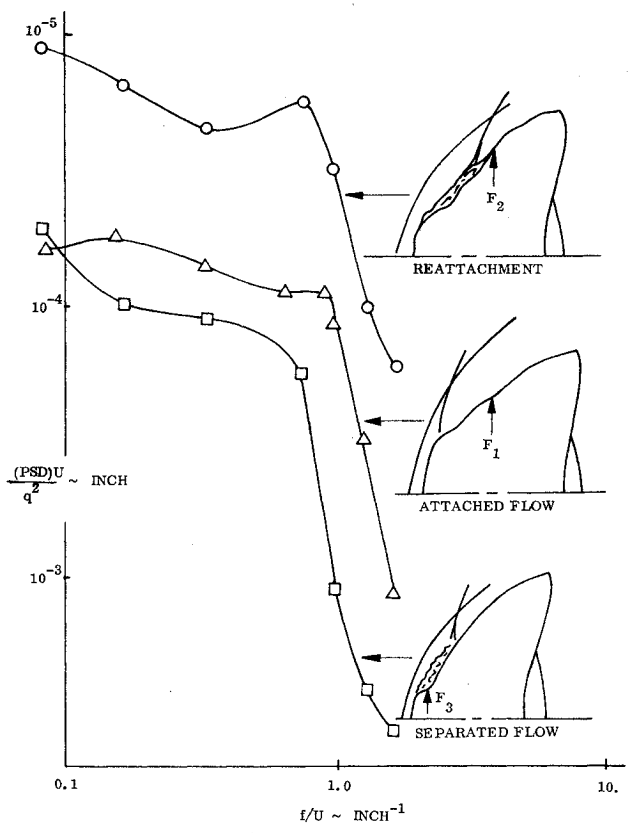

Fig. 18 Comparison of spectra, LTA smooth, $R_e = 40 \times 10^6$/ft, $\alpha = 0$ deg, $M = 5.0$.

the turbulent spectra is significantly greater. If the lifted boundary layer over a region of separated flow is similarly affected by transition, this could indeed be indicative of transitional separation.

The shape of the spectra on a blunt conic nosetip (model 2) is distinctly different from either the separated flow or reattachment spectra on the indented nosetip (model 4) although the level is roughly intermediate between the two (compare Figs. 16 and 17). Conversely, there is a strong similarity in the shape of the spectra on the blunt conic meridian, the $\phi = 0$-deg meridian, of the smooth LTA replica and the spectra under flow reattachment on the adjacent indented region at $\phi = 60$ deg (Fig. 18). The separated flow at $\phi = 60$ deg is somehow affecting the flow over the blunt conic section at $\phi = 0$ deg. This supports the contention that the reattachment shock extends laterally over the $\phi = 0$-deg meridian and is indeed responsible for the static pressure peak observed there (Fig. 13).

A Reynolds number sensitive resonant peak also appears in the reattachment spectra for the replica NRV nosetip for transducer F_1 at the $\phi = 310$-deg azimuth (Fig. 19). No similar peak was observed for the F_3 transducer at the 188-deg azimuth. The spectral peak at $\phi = 310$ deg is believed to be the result of a longitudinal vortex shed from the ridge adjacent to transducer F_1 (see inset sketch in Fig. 19). The peak shifts with Reynolds number, moving to lower semi-normalized frequencies at higher Reynolds number. The width of the peak is about the same for $R_e = 10 \times 10^6$/ft and $R_e = 40 \times 10^6$/ft. The log scale of f/U makes the higher frequency peak appear narrower.

The semi-normalized reattachment spectra and/or the spectra under the imbedded shocks (model 2) show diverse levels although the spectra shapes are similar. All have identical rolloff characteristics. That is, the power spectra all decrease at the same rate at high semi-normalized frequencies (Fig. 20; spectra showing flow resonance effects have been excluded from this comparison). The similarity of the shapes of the reattachment spectra is better illustrated in Fig. 21, where the spectra are nondimensionalized with the maximum height of the separated flow regions δ_m, and the area under

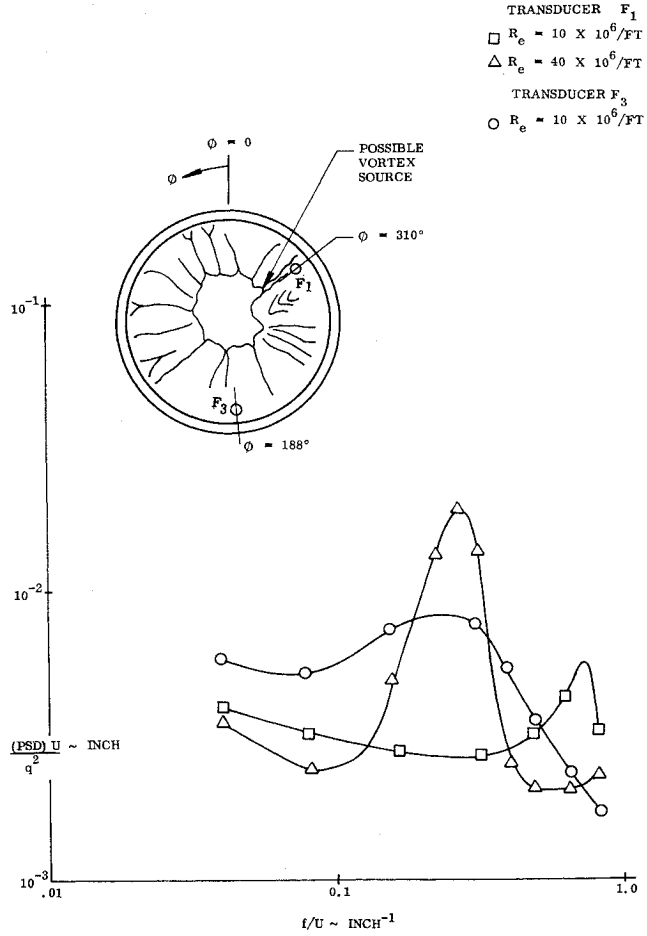

Fig. 19 Reattachment spectra, NRV nosetip.

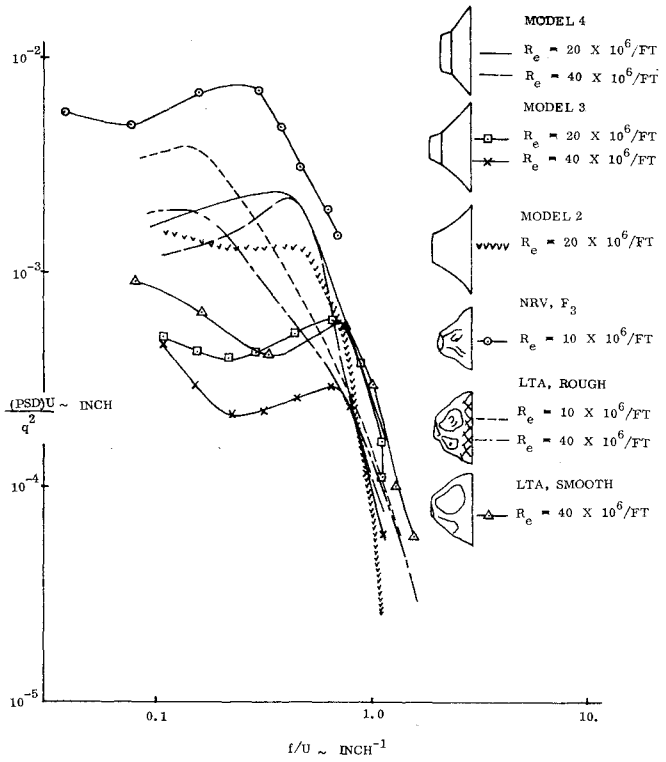

Fig. 20 Comparison of semi-normalized reattachment spectra.

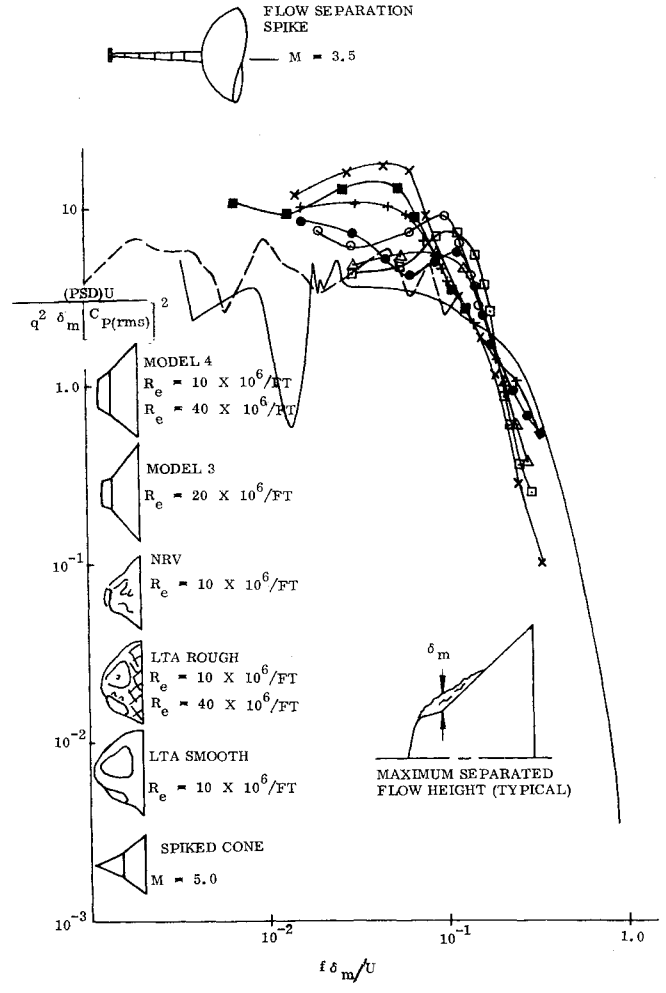

Fig. 21 Comparison of nondimensionalized reattachment spectra.

the nondimensional spectra $(C_{P(\text{rms})})^2$ which eliminates amplitude effects caused by local static pressure differences.

δ_m was measured from the body surface in a direction normal to the body centerline to the top of the separated region as defined by shadowgraph photographs. Where shadowgraph photographs did not reveal the separated flow boundary (as for the replica models), or where they were unavailable (as for the spiked cone data[3]) the separated flow boundary was assumed to be a straight line from the shoulder of the laminar cap or from the spike apex to the pressure peak at reattachment. Using the separated flow height to nondimensionalize the spectra was first suggested by Coe and Chyu.[14] By using the maximum separated flow height δ_m, one is essentially scaling the spectra to the maximum possible eddy size of the particular region of separated flow. The collapse of the data into nearly a single curve (Fig. 21) indicates a similar partition of energy, as a function of eddy size, for a variety of spike-induced separated flows (e.g., for mildly and severely indented noses, and for a flow separation spike). This suggests a universal, nondimensional, spectral shape for reattaching flow separation which could form the basis of an emperical prediction technique when combined with correlations of the overall fluctuating pressure levels (as in Figs. 14 and 15) and the separated flow geometry.

Conclusions

Fluctuating pressure measurements on a variety of turned (axisymmetric) and cast replica models simulating mildly indented, ablated, re-entry body nosetips have been analyzed. The analysis has shown that reattaching flow separation produces the most severe fluctuating pressures on the nosetip. Furthermore, the effect of surface irregularities typical of a flight recovered nosetips, were significant. They not only affected the environment locally but caused significant perturbations at other circumferential and axial (downstream) stations. Particularly large, Reynolds number sensitive, resonant peaks were observed in the reattachment spectra. Until these effects are well understood it is recommended that the surface irregularities be simulated in ground tests in order to properly predict the flight environment.

A technique of collapsing the power spectra in regions of flow reattachment is presented. The good correlation of the reattachment spectra for a variety of configurations suggests a universal, nondimensional, spectra shape for reattaching flow separation. This seems to be a promising area for future work as it could form the basis of an empirical technique for predicting the fluctuating pressure environment in regions of flow reattachment.

Acknowledgments

The author wishes to express his appreciation to R. T. Driftmyer, Naval Surface Weapons Center, who conducted the wind-tunnel tests and supervised the data reduction.

References

[1] Wallace, G. A., "Wind Tunnel Test Series Conducted for LMSC, Part I Low Temperature Scallop Formation and Growth Data," Acurex Corporation/Aerotherm Division, Mt. View, Calif., Aerotherm Rept., 75-147, June 1973.

[2] Otey, G. R. and English, E. A., "High-β Re-entry Vehicle Recovery," *Journal of Spacecraft and Rockets,* Vol. 14, May 1977, pp. 290-293.

[3] Baltakis, F. P., "Wind-Tunnel Study of Oscillating Flow-Induced Surface Pressures on a Tension-Cone Geometry Model," Naval Ordnance Laboratory, White Oak, Md., Technical Rept. NOL TR 74-134, Jan. 1974.

[4] Wood, C. J., "Hypersonic Flows over Spiked Cones," *Journal of Fluid Mechanics,* Vol. 12, April 1962, pp. 614-624.

[5] Kabelitz, H. P., "Zur Stabilitat Geschlossener Grenzch: Chtablosegebiete on Konischen Drehkorpen bi," Hyperschallen Stromung, DLD FB 71-77, July 1972.

[6] Abbett, M. J., Cooper, L., Dahm T. J., and Jackson, M. D., "Unsteady Flow on Ablated Nosetip Shapes," Pant Series G, Test

and Analysis Rept., Acurex Corp./Aerotherm Div., Mt. View, Calif., Aerotherm Rept. 73-87, Dec. 1973.

[7]Baltakis, F. P., "Performance Capability of the NOL Hypersonic Tunnel," U. S. Naval Ordnance Laboratory, White Oak, Md., NOLTR 68-157, Oct. 24, 1968.

[8]Driftmyer, R. T., Regan, F. J., and Ragsdale, W. C., "Summary of the R198 LN Pressure Wind Tunnel Test Program, Mach 5 and 9," Naval Surface Weapons Center, White Oak Laboratory, Wind-Tunnel Rept. No. 121, Jan. 1977.

[9]Driftmyer, R. T., Regan, F. J., and Ragsdale, W. C., "Summary of the R198 Replica and Smoothed Model Wind-Tunnel Test Program, Mach 5 and 9," Naval Surface Weapons Center, White Oak Laboratory, Wind-Tunnel Rept. No. 120, Jan. 1977.

[10]Ragsdale, W. C., Knott, J., and Regan, F. J., "Summary of the R-198 LN Static Force Wind-Tunnel Program," Naval Surface Weapons Center, White Oak Laboratory, Wind-Tunnel Rept. No. 116, Dec. 1976.

[11]Jackson, M. P. and Baker, D. L., "Interim Report Passive Nosetip Technology (PANT) Program, Vol. III Surface Roughness Effects, Part I, Experimental Data," Aerotherm Division/Acurex Corp., Mt. View, Calif., Aerotherm Rept. 74-90; also SAMSO-TR-86, Vol. III, Pt. I, Jan. 1974.

[12]Holden, M. S., "Studies of the Effects of Transitional and Turbulent Flows on the Aerodynamic Performance of Re-entry Vehicles in Hypersonic Flows," Calspan Corp., Buffalo, N. Y., Calspan Rept. HB-5834-A-2, April 1978.

[13]Seiff, A., "Secondary Flow Fields Imbedded in Hypersonic Shock Layers," NASA TN D-1304, 1962.

[14]Coe, C. F. and Chyu, W. J., "Pressure Fluctuation Inputs and Response of Panels Underlying Attached and Separated Supersonic Turbulent Boundary Layers," NASA TM X-62, 189, Sept. 1972.

[15]Chyu, W. J. and Hanly, R. D., "Power and Cross-Spectra and Space-Time Correlations of Surface Fluctuating Pressures at Mach Numbers Between 1.6 and 2.5," AIAA Paper 68-77, AIAA 6th Aerospace Sciences Meeting, New York, N. Y., June 1968.

[16]Guenther, R. A. and Reding, J. P., "Fluctuating Pressure Environment of a Drag Reduction Spike," *Journal of Spacecraft and Rockets,* Vol. 14, Dec. 1977, pp.705-710.

[17]Reding, J. P., Guenther, R. A., and Jecmen, D. M., "Scale Effects on the Fluctuating Pressures in a Region of Spike-Induced Flow Separation, "AIAA Paper 79-0143, AIAA 17th Aerospace Sciences Meeting, New Orleans, La., Jan. 1979.

[18]Garcia, F. S., "Fluctuating Pressure Measurements on the Apollo Boiler Plate of Saturn Vehicles SA-6 and SA-7," private communication, June 1965.

[19]Ericsson, L. E., "Flow Oscillations on Concave Forebodies," AIAA Paper 77-1130, AIAA Atmospheric Flight Mechanics Conference, Hollywood, Fla., Aug. 1977.

[20]Martellucci, A., Chaump, L., Rodgers, D., and Smith, D., "Experimental Determination of the Aeroacoustic Environment About a Slender Cone," *AIAA Journal,* Vol. 11, May 1973, pp. 635-641.